Journal of Power Technologies 100 (3) (2020) 223–231

Multi-Criteria Assessment of Injector Placement and the Thermodynamic Effects of Fuel Injection and Combustion in an Engine Equipped with Direct Gasoline Injection System

Ireneusz Pielecha [*], Maciej Sidorowicz [†]

Abstract

The paper concerns the analysis of the combustion and exhaust emission phenomena in an SI (spark ignition) engine equipped with direct gasoline injection system for various injector placement parameters in the combustion chamber. Achieving a good combustion process is shaped by the direct fuel injection process, of which parameters vary. This article focuses on the aspect of injector spatial and angular position in order to perform injection and achieve fuel combustion. The injector's pseudo-optimal location has been presented along with several changed positions (27 configurations). The research was conducted as a simulation experiment using AVL FIRE software. The best injector position was selected based on the fuel atomization, injection and combustion process indicators. The pseudo-optimal location, was characterized by: 1) the largest inset in the combustion chamber: $y = 7$ mm, 2) the shortest distance from the spark plug: $z = 9$ mm, 3) the highest angle in relation to the axis of the cylinder: alpha $= 20$ deg. The analysis of this impact results in the following conclusions: 1) the longitudinal change of the injector position is the most important value affecting changes in the fuel atomization and combustion indicators, 2) this change is about 3 times more significant than the change in the position of the injector's distance from the axis of the spark plug and about 8 times more significant than the angle of the injector's position.

Keywords: Gasoline direct injection, Fuel combustion, Simulation of combustion

1 Introduction

Gasoline direct injection is a solution that is currently very rapidly replacing indirect injection technology in spark ignition engines. The share of these injection systems in new vehicles equipped with SI engines in the US market increased in the years 2009-2015 from 5% to 46%. It is believed that the share of these engines in all on-road vehicles will reach over 50% by 2020 Zimmerman et al. (2016).

*Poznan University of Technology e-mail
†Poznan University of Technology e-mail

There are various ways of shaping the fuel stream during direct injection Pielecha (2014), but all are aimed at creating a stoichiometric mixture in the vicinity of the spark plug, at the moment of discharge on its electrodes.

One of the methods of shaping the fuel injection stream is the spray-guided method Pielecha (2014), which consists of injecting liquid fuel in such a way that the fuel stream creates a stoichiometric mixture in the vicinity of the spark plug without interacting with any other factor aside from air.

Generally, a central position of the spark plug in the combustion chamber is preferred: it allows a symmetrical propagation of the flame front initiated by the spark, taking a shorter path to extend combustion to the whole unburned mixture and more likely reaching it before auto-ignition occurs Fiengo et al. (2012).

Injection tests were carried out by Zulkefli and Mansor (2015) in relation to hydrogen direct injection. It was found that the best injector position for such application in an internal combustion engine is the position at 0° from the combustion chamber axis: it gives the largest mixing area and effective mass diffusivity of air and the flame can propagate uniformly for the entire combustion process.

The influence of the CNG and H_2 injectors position change in the intake manifold was studied by Chintala and Subramanian (2013). It has been found that a proper injector location allows for a turbulence change of over 50%.

The impact of the methanol injector placement in a dual-fuel engine (diesel-methanol) was studied by Chen et al. (2017). It was found that only the maximum engine load affects changes in the emission value. The influence of the methanol contribution to NO_x emission was low: no changes were noted in relation to the other injector positions, and with increasing the proportion of methanol – there was a decrease in NO_x emissions.

Yan et al. (2018) analyzed the influence of the combustion chamber geometry on the injection and com-

bustion processes in an engine powered with the natural gas. Altin and Bilgin (2015) in the research on the various spark plug locations inside the combustion chamber remarked on the cylinder pressure, temperature, heat losses, combustion process duration and burned fuel mass. Ravi and Porpatham (2017) took up the subject of the impact of the piston shape on the performance and exhaust emission in an engine powered with the LPG operating at full power. Gonca (2017) compared brake power, brake thermal efficiency and NO emission using different fuels with changing the engine bore and stroke. Gupta and Mittal (2019) investigated the influence that the compression ratio has on the performance and exhaust emission in an engine powered with bio-methane. Nazemian et al. (2019) analyzed the heat recuperation possibilities in an RCCI engine with the changes of piston geometry and injection strategy. Despite many of the described aspects of the quoted research on the combustion chamber geometry and the mutual placement of the spark plug and injectors, there are still few publications exhaustively analyzing the injection and combustion processes or exhaust emission, depending on the geometrical conditions of the combustion chamber of an SI engine powered with direct gasoline injection.

The research on the combustion process conducted on real engines incur higher financial and material costs compared to similar research using the CFD techniques. The initial design phase of a combustion system is usually connected to a simulation project (Ahmadi and Hosseini (2018),Krishnaraj et al. (2017),Ranga et al. (2017),Wiemann et al. (2018)). In spite of this approach, the final result verification is still conducted on real engines (Akansu et al. (2017),García-Morales et al. (2017),Liu et al. (2018),Su et al. (2018)).

The aim of the research is to find the optimal spatial injector location relative to the spark plug and the angular position relative to the cylinder axis. The sum of the thermodynamic indicators concerning the combustion process and the exhaust emission should reach the highest value, while also meeting the arbitrarily set assumptions and the weighed contributions.

The described research is motivated by the need of initial verification of the injection and combustion effectiveness increase in a double direct injection system. Before designing the real model of such system, the geometrical conditions must be defined within the boundary conditions, so the injection and combustion processes progress most effectively.

2 Research methodology

2.1 Combustion chamber geometry

The research on the combustion process was performed using the AVL Fire 2017.1 simulation software. The shape of the combustion chamber was modelled, so it corresponds to the real chamber of the 1-cylinder internal combustion engine (Fig. 1). The movable mesh of a linear dimension having a value of 1 mm was automatically refined in the area of a spark plug down to the value of 0.1 mm. The engine technical parameters was presented in Table 1. Every injector location was described with the code containing the changes in the y-axis position, the z-axis position and the angle in relation to the cylinder axis:

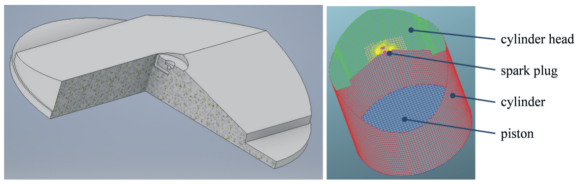

Figure 1: Combustion chamber with the considered spark plug: a) 3D model, b) mesh implemented in AVL Fire

Parameter	Unit	Value
Type	–	piston engine, 4-stroke, SI
Cylinder number	–	1
Displacement	cm^3	385
Compression ratio	–	10.2
Bore	mm	83
Stroke	mm	71.2
Start of injection*	deg	670
Injection duration	ms	0.6
Injected fuel mass	mg	13.1
Excess air ratio	–	1.5
Ignition crank angle	deg	690

Table 1: Modelled engine technical data (* in the whole research, the 0 deg crank angle corresponds to the top dead center preceding power stroke)

$$y(i)z(j)alpha(k)$$

where: i = 7, 8 and 9 mm, j = 9, 10 and 11 mm, k = 15, 17.5 and 20 deg.

The research was done using 27 injector placement configurations (Fig. 2 and Fig. 3).

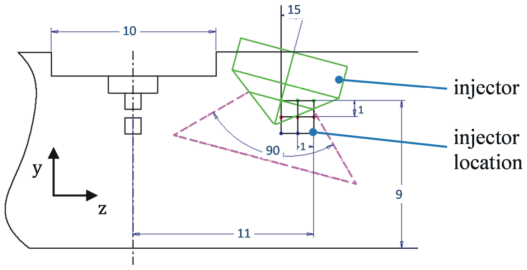

Figure 2: Configuration of the combustion process tests concerning the linear and angular injector's position change

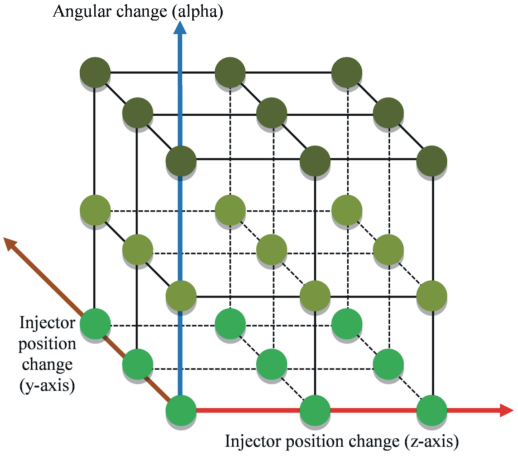

Figure 3: The injection and combustion process research with injector's placement variants

2.2 Modeling the fuel injection

Fuel injection started at an angle of 670 deg and lasted $t = 0.6$ ms. The fuel dose was 13.1 mg, which corresponded to the excess air ratio value of lambda = 1.5.

Fuel injection is based on the atomization of droplets, based on the KHRT model. Some authors Kosmadakis et al. (2015) use this model to study direct injection of gasoline from multi-hole injectors supplied at a pressure of 7.5–12 MPa. Due to the omission of gravity and viscous forces in this model Ghadimi et al. (2016), it is commonly used for numerical shaping of the high velocity stream injection. The validity of using the above model for a hollow cone-shaped stream has been verified many times before Reitz and Beale (1999).

2.3 Initial conditions of combustion

The initial conditions of the compression process and the combustion process were adopted in accordance with the values listed in Table 2. Such conditions correspond to a spark-ignition engine with direct fuel injection at the speed of 2000 rpm.

Parameter	Value
Pressure	0.6 bar
Temperature	300 K
TKE	10 m^2s^{-2}
Turb. diss. rate	1732.05 m^2s^{-3}
Tumble rotational speed	3000 rpm
Engine speed	2000 rpm
Crank angle	570-800 deg. CA
Atomization	KH-RT model
Evaporation model	Dukowicz evaporation model
Combustion modelling	Extended Coherent Flame Model
NO formation	Zeldovich extended
Soot formation	Kinetic Soot Model

Table 2: Initial conditions adopted for the combustion process simulation calculations

2.4 Modeling of the combustion process and exhaust emission

The pre-combustion conditions inside the combustion chamber were determined according to the process described in Sidorowicz and Pielecha (2018). The with the spherical shape of the initial flame nucleus was adopted for the combustion simulation calculations.

All the required radicals for Zeldovich extended NO formation model are calculated based on the equilibrium approach, which assumes that the residence time is short Maroteaux and Saad (2015), known and used in the ECFM combustion model (mentioned above).

Tan et al. (2016) acknowledged that multi-step semi-empirical models provide a relatively complete characterization of soot processes at affordable computational cost and effort, considering the trade-off between accuracy and applicability.

3 Impact of injector placement on fuel atomization conditions

Various injector positions were analyzed in terms of changes in: mass of evaporated fuel, mass of remaining (unevaporated) fuel, diameter of fuel droplets, turbulence kinetic energy, dissipation of energy and excess air ratio.

Figure 4 presents the results of fuel atomization analysis taking into account the change of the injector's position in the direction of the y axis (according to Fig. 2 and Fig. 3).

The most advantageous position is far in the combustion chamber (reduction of the y coordinate). In this

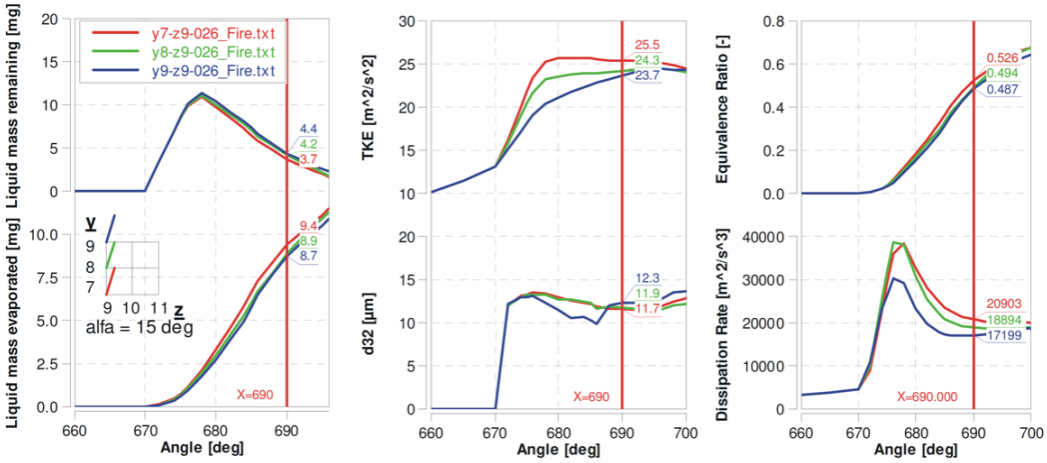

Figure 4: Impact of the injector position change in the combustion chamber – y coordinate (changes in the injector placement height in the combustion chamber)

position (value $y = 7$ mm), the amount of the vaporized fuel is the highest at a constant crankshaft angle (analysis was done for the ignition point – at the angle of 690 deg). This injector position prevents the fuel stream from reaching the spark plug electrode which improves fuel evaporation. The extreme positions of the injector along the variable y (position changes in relation to the cylinder axis) relative to the solution adopted ($y = 7$ mm) result (at a crankshaft angle of 690 deg) in:

- increasing the evaporated fuel mass by 7.4%;
- decreasing the unevaporated fuel mass by 18.9%;
- reducing the droplet diameter by 2.6%;
- increasing the turbulence kinetic energy by 7.1%;
- increasing the energy dissipation by 17.7%;
- increasing the excess air ratio by 7.5%.

Changes in the position of the injector relative to the z axis (distance from the spark plug) do not lead to such large differences in the analyzed indicators. The best solution is the location ($z = 9$ mm at an angle of 690 deg), because the evaporated fuel mass is the largest.

4 Comparative analysis of the injector placement in the combustion chamber

First, the mass of evaporated fuel was determined for all injector positions relative to the angle of its location (Fig. 5a) at the engine's crankshaft angle of 690 deg. The comparison indicates that the largest mass of evaporated fuel does not occur at the same injector position at each one of its placement angles. The highest values of evaporated fuel were obtained at the location coordinates of $y(7)z(9)$alpha(15) and $y(7)z(9)$alpha(20) – which means $y = 7$ mm and $z = 9$ mm at the angles of 15 and 20 deg. However, at an angle of 17.5 deg, the best option was to place the injector at the coordinates $y = 7$ and $z = 11$ (code $y(7)z(9)$alpha(17.5)).

Analysis of the average excess air ratio in the combustion chamber (at an angle of 690 deg) shows similar tendencies (Fig. 5b) to previous considerations. The largest values of the global excess air ratio were obtained for the same settings.

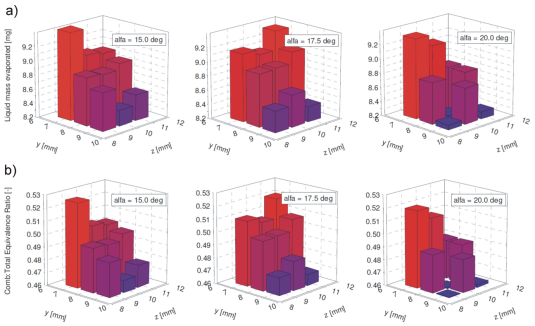

Figure 5: Changes in fuel atomization indicators: a) weight of evaporated fuel, b) equivalence ratio (1/lambda) at various injector positions in the combustion chamber

5 Impact of injector placement on the combustion process

5.1 Combustion process thermodynamic indicators

The thermodynamic indicators chosen for the quantitative analysis of the combustion process were: the average combustion temperature, the average combustion pressure, the heat release rate (based on e.g. Petrakides et al. (2018)) and the total heat released in the combustion process.

Changes in the position of the injector relative to the z axis (distance from the spark plug) do not lead to such large changes in the analyzed indicators (Fig. 6). The best solution for the assumed values of other parameters (y = 7 mm, alpha = 15 deg) is the location (z = 10 mm), which does not confirm the fuel spray analysis results described in Sidorowicz and Pielecha (2018). Three out of four indicators have the highest value for this position. Comparing this solution of the z axis position (z = 10 mm) with the position which give the least favourable indicator values (z = 11 mm) result in:

- increasing the mean temperature by 1.6%;
- increasing the mean pressure by 4.1%;
- increasing the rate of heat release by 1.2%;
- increasing the total heat released by 0.9%.

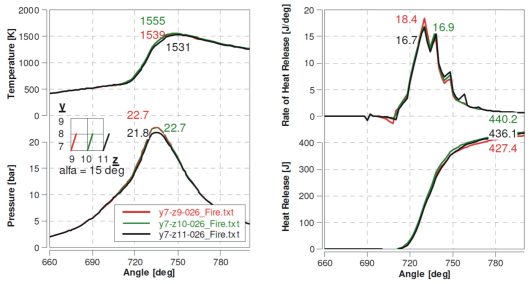

Figure 6: Impact of the injector position change on the combustion process indicators - coordinate z (changes of the injector distance from the spark plug in the combustion chamber)

5.2 Combustion process emission indicators

Complementing the combustion process analysis in relation to the geometric parameters of the injector location in the combustion chamber, the exhaust emission testing was carried out (the concentration of exhaust components was used because all the results are taken for the same one point of engine operation). Four indicators were used: nitrogen oxide emission, soot emission, carbon dioxide emission and carbon monoxide emission. Minimum CO and soot emission values as well as maximum values of NO and CO_2 emissions were deemed as the most desirable.

It was assumed that increasing the NO concentration indicates a more favorable combustion process, despite the fact that the NO concentration is undesirable. The reduction of NO emissions, however, was not the main goal of this research.

Figure 7 indicates that the change in the alpha angle (injector position) mostly affects the concentration of soot and carbon monoxide. This is due to the preparation of the mixture in the initial combustion phase, where the proportion of oxygen that can react with the hydrocarbon molecules in the fuel around the spark plug is insufficient to ensure complete combustion.

Analysis of the injector angular position with respect to the cylinder axis in relation to the exhaust emissions (with a fixed linear position of the injector tip for y = 7 mm, z = 9 mm) does not yield unambiguous results for optimal placement of the injector inside the combustion chamber. Comparison of the angular position 20 deg with respect to the alpha = 15 deg position results in the following changes (Fig. 7):

- increasing the NO concentration by 33.7%;
- increasing the soot concentration by 160.3%;
- increasing the CO_2 concentration by 3.5%;
- decreasing the CO concentration by 5.3%.

The next stage of the research work was the spatial analysis of selected emission factors. The following is the distribution of NO concentration and soot in the combustion chamber. Analysis of the 3D results of the exhaust gas components formation indicates that the angular injector position has a large impact on the intermediate states of nitrogen oxide and soot formation (Fig. 8 and 9). This means that the average values presented in Fig. 7 do not allow making a full assessment of the formation of compounds during combustion.

The next stage of the research work was the spatial analysis of selected emission factors. The following is the distribution of NO concentration and soot in the combustion chamber. Analysis of the 3D results of the exhaust gas components formation indicates that the angular injector position has a large impact on the intermediate states of nitrogen oxide and soot formation (Fig. 8 and 9). This means that the average values presented in Fig. 7 do not allow making a full assessment of the formation of compounds during combustion.

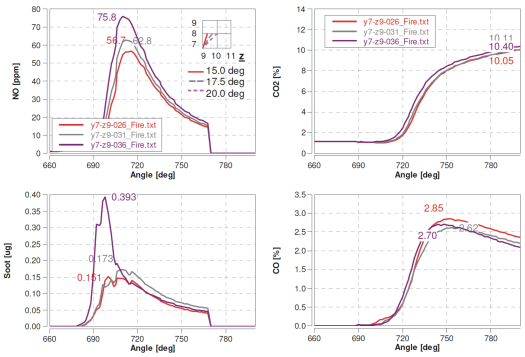

Figure 7: Impact of the injector position change in the combustion chamber on emission factors – alpha angle (injector position)

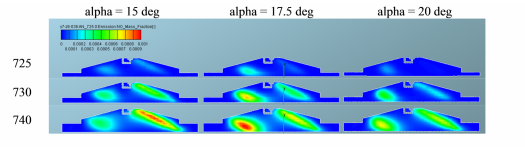

Figure 8: Distribution of NO concentration during combustion with the injector positioned at $y = 7$ mm, $z = 9$ mm and alpha = 15 deg, alpha = 17.5 deg, alpha = 20 deg respectively

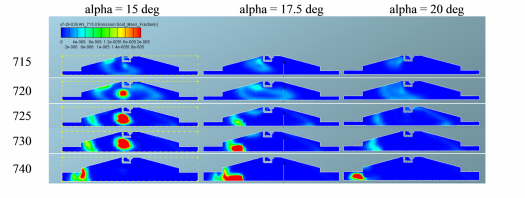

Figure 9: Distribution of spatial formation of soot during combustion with the injector positioned at y = 7 mm, z = 9 mm and alpha = 15 deg, alpha = 17.5 deg, alpha = 20 deg respectively

6 Evaluation of the combustion process from the perspective of combustion indicators – selection of the best configuration

These considerations prompted the authors to determine the best injector position through pseudo-optimization. With the obtained values of maximum cylinder pressure, maximum cylinder temperature, total heat released, CO, CO_2 and NO emission, and soot formation, the data was scaled.

Thus the following values have been used:

- the best value for a given indicator to take (the largest mass of evaporated fuel, smallest droplet diameter, the smallest energy dissipation, the largest TKE, the smallest equivalence ratio – the largest value of excess air ratio and the highest temperature of the fuel dose, the highest cylinder temperature, the highest cylinder pressure, the largest heat released, the largest CO and NO concentration, the smallest CO fraction and the smallest formed soot factor) that can be obtained is equal to 1;
- the worst possible indicator value is 0.

The scaling was performed on this basis, and the results are presented in Fig. 10. The values of particular indicators have been assigned to each of the injector's positions. Figure also contains a pictogram analysis, which shows that the most positive results occur when placing the injector at the coordinates $y = 7$ mm and $z = 9$ mm or $z = 10$ mm. The worst position of the injector is the one with the y coordinate of $y = 9$ mm.

Due to the fact that it was still impossible to determine the best injector position, the normalized values of process indicators were summed for each of the injector positions. Using such a summation method, the maximum possible value is 13. The highest value of 10.07 normalized indicators was obtained for the injector position with the coordinates $y = 7$, $z = 9$ and the angle alpha = 20 deg (code: $y(7)z(9)$alpha(20)), as shown in the column titled "Index" in Fig. 10. It should be noted, however, that the values do not show any tendency of the injector positioning based upon the used indicators, as it took place in spray analysis (Sidorowicz and Pielecha (2018)).

Additionally, in Fig. 11, the sums of normalized combustion indicators are summarized (sum of the "Index" column for individual injector positions). They were calculated using:

$$y(7mm) = \sum y(7)z(j)alpha(k)$$

$$y(8mm) = \sum y(8)z(j)alpha(k)$$

$$y(9mm) = \sum y(9)z(j)alpha(k)$$

$$z(9mm) = \sum y(i)z(9)alpha(k)$$

$$z(10mm) = \sum y(i)z(10)alpha(k)$$

y	z	alfa	Liq. mass rem.	d32	Dissip. rate	TKE	Equiv. ratio	Temperature	Pmax	Tmax	HRmax	CO2-max	NO-max	CO-min	Soot-min	Index	Index
mm	mm	deg	kg	m	m^2/s^3	m^2/s^2	-	K	Pa	K	J	-	-	-		[-]	%
7	9	15	✓ 1.00	! 0.43	✓ 1.00	✓ 0.99	✓ 1.00	✗ 0.00	! 0.42	✓ 0.71	! 0.62	! 0.63	✗ 0.18	✗ 0.07	✓ 1.00	⇨ 8.05	61.9
		17.5	✓ 0.76	! 0.56	✓ 0.91	✓ 0.94	✓ 0.76	✗ 0.30	! 0.46	✓ 0.67	✓ 0.72	✓ 0.68	✗ 0.32	✗ 0.29	✓ 0.84	⇧ 8.23	63.3
		20	✓ 0.91	! 0.51	✓ 0.99	✓ 1.00	✓ 0.91	✗ 0.19	✓ 1.00	✓ 1.00	✓ 0.82	✓ 0.93	! 0.61	✗ 0.21	✓ 0.99	⇧ 10.07	77.5
	10	15	✓ 0.68	✗ 0.29	! 0.66	! 0.60	✓ 0.68	✗ 0.26	! 0.41	✓ 0.80	✓ 0.81	✓ 0.82	! 0.44	✗ 0.07	✓ 0.98	⇨ 7.48	57.6
		17.5	✓ 0.70	✗ 0.32	✓ 0.74	✓ 0.73	✓ 0.70	✗ 0.33	! 0.42	✓ 0.93	✓ 1.00	✓ 1.00	✗ 0.32	✗ 0.26	✓ 0.86	⇧ 8.32	64.0
		20	✓ 0.77	✗ 0.32	✓ 0.79	✓ 0.79	✓ 0.77	✗ 0.28	! 0.34	! 0.52	! 0.57	✓ 0.71	! 0.55	✗ 0.23	✓ 0.93	⇨ 7.57	58.3
	11	15	! 0.65	✗ 0.19	! 0.56	! 0.46	! 0.65	✗ 0.28	✗ 0.21	✓ 0.67	✓ 0.75	✓ 0.69	! 0.52	✗ 0.16	✓ 0.89	⇨ 6.67	51.3
		17.5	✓ 0.93	! 0.37	! 0.60	! 0.55	✓ 0.93	✗ 0.11	✗ 0.15	! 0.59	✓ 0.67	✓ 0.72	✗ 0.31	✗ 0.03	✓ 0.92	⇨ 6.89	53.0
		20	! 0.46	✗ 0.32	! 0.66	✓ 0.68	! 0.46	! 0.54	✗ 0.28	! 0.61	✓ 0.72	✓ 0.71	✗ 0.18	! 0.49	✓ 0.83	⇨ 6.95	53.4
8	9	15	! 0.52	! 0.37	! 0.48	! 0.33	! 0.52	! 0.40	✗ 0.14	! 0.52	! 0.61	! 0.64	✗ 0.00	✗ 0.00	✓ 0.97	⇩ 5.51	42.4
		17.5	! 0.58	✗ 0.31	! 0.49	! 0.35	! 0.58	! 0.47	! 0.48	✓ 0.81	✓ 0.87	✓ 0.90	✗ 0.30	✗ 0.32	✓ 0.97	⇨ 7.43	57.2
		20	! 0.45	! 0.43	! 0.45	! 0.36	! 0.45	✓ 0.67	! 0.62	! 0.51	! 0.41	! 0.51	✓ 1.00	✓ 0.67	✓ 0.97	⇨ 7.51	57.8
	10	15	! 0.51	! 0.41	! 0.43	✗ 0.31	! 0.51	! 0.43	✗ 0.24	! 0.66	✓ 0.67	✓ 0.88	✓ 0.79	✗ 0.20	✓ 0.98	⇨ 7.03	54.1
		17.5	! 0.60	✗ 0.33	! 0.42	! 0.34	! 0.60	! 0.44	✗ 0.25	! 0.61	! 0.58	✓ 0.75	✗ 0.22	! 0.54	✓ 0.95	⇨ 6.61	50.8
		20	✗ 0.00	✗ 0.00	! 0.42	! 0.38	✗ 0.00	✓ 0.90	! 0.52	✓ 0.71	✓ 0.70	✓ 0.75	✓ 0.72	! 0.41	✓ 0.85	⇨ 6.36	48.9
	11	15	! 0.59	✗ 0.24	! 0.33	✗ 0.29	! 0.59	✗ 0.28	! 0.36	✓ 0.72	✓ 0.69	✓ 0.75	✗ 0.12	✗ 0.09	✓ 0.86	⇩ 5.91	45.5
		17.5	✓ 0.73	✗ 0.21	✗ 0.33	✗ 0.29	✓ 0.73	✗ 0.20	✗ 0.29	! 0.58	! 0.63	✓ 0.73	! 0.62	✗ 0.18	✓ 0.91	⇨ 6.44	49.5
		20	! 0.46	✗ 0.26	✗ 0.32	! 0.33	! 0.46	! 0.55	✗ 0.32	! 0.56	! 0.65	✓ 0.68	! 0.40	! 0.52	! 0.59	⇩ 6.10	46.9
9	9	15	! 0.41	✗ 0.24	✗ 0.04	✗ 0.01	! 0.41	! 0.62	✗ 0.15	! 0.38	! 0.39	! 0.46	✗ 0.08	! 0.41	! 0.67	⇩ 4.27	32.8
		17.5	✗ 0.21	✓ 0.73	✗ 0.00	✗ 0.00	✗ 0.21	✓ 0.86	! 0.64	! 0.57	! 0.54	! 0.60	✓ 0.82	! 0.65	✓ 0.79	⇨ 6.63	51.0
		20	✗ 0.01	✓ 1.00	✗ 0.00	✗ 0.10	✗ 0.01	✓ 1.00	✗ 0.10	✗ 0.00	✗ 0.00	✗ 0.00	! 0.53	✓ 1.00	✓ 0.91	⇩ 4.67	35.9
	10	15	✗ 0.15	✗ 0.17	✗ 0.04	✗ 0.08	✗ 0.15	✓ 0.75	✗ 0.00	✗ 0.33	✗ 0.22	! 0.49	✓ 0.72	! 0.50	✓ 0.79	⇩ 4.36	33.6
		17.5	! 0.34	✗ 0.23	✗ 0.04	✗ 0.13	! 0.34	✓ 0.68	! 0.36	! 0.54	! 0.54	! 0.60	! 0.53	! 0.61	✓ 0.81	⇩ 5.76	44.3
		20	! 0.39	✓ 0.77	✗ 0.03	✗ 0.17	! 0.39	✓ 0.72	✗ 0.31	! 0.44	! 0.48	! 0.50	! 0.60	! 0.52	✓ 0.87	⇨ 6.19	47.7
	11	15	✗ 0.27	✗ 0.15	✗ 0.07	✗ 0.17	✗ 0.27	! 0.57	✗ 0.22	✓ 0.71	! 0.64	✓ 0.91	! 0.49	✗ 0.03	✓ 0.81	⇩ 5.32	40.9
		17.5	✗ 0.14	✗ 0.12	✗ 0.06	✗ 0.23	✗ 0.14	✓ 0.70	! 0.45	! 0.60	! 0.42	✓ 0.70	✓ 0.78	! 0.37	✓ 0.70	⇩ 5.42	41.7
		20	✗ 0.04	✗ 0.24	✗ 0.06	✗ 0.28	✗ 0.04	✓ 0.85	! 0.56	! 0.39	✗ 0.18	✗ 0.28	! 0.48	✓ 0.79	✗ 0.00	⇩ 4.20	32.3

Figure 10: Relative values of fuel combustion rates and of exhaust components concentration at individual injector positions

$$z(11mm) = \sum y(i)z(11)alpha(k)$$

$$alpha(15\,\mathrm{deg}) = \sum y(i)z(j)alpha(15)$$

$$alpha(17.5\,\mathrm{deg}) = \sum y(i)z(j)alpha(17.5)$$

$$alpha(20\,\mathrm{deg}) = \sum y(i)z(j)alpha(20)$$

where: $i = 7$, 8 and 9 mm, $j = 9$, 10 and 11 mm, while $k = 15$, 17.5 and 20 deg.

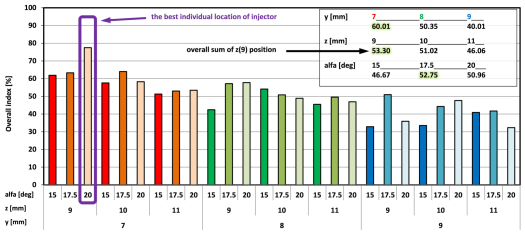

Figure 11: Indicators of the best injector position selection based on selected parameters related to fuel injection conditions and its combustion (based on Fig. 10)

The performed comparison leads to the conclusion that the highest point value was obtained for the injector positions with $y = 7$ mm. This means that combustion indicators take the highest values at this injector setting, regardless of the other position variables. This position, selected for the variable z, is $z =$

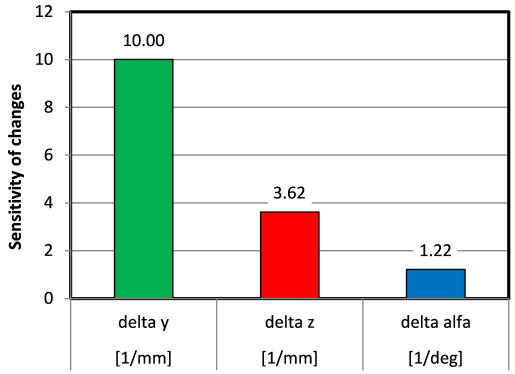

Figure 12: Sensitivity of changes in the parameters y, z and angle of the injector to the conditions of injection and fuel combustion process

9 mm. Although the best individual angular position turned out to be 20 deg (code $y(7)z(9)$alpha(20) – at $y = 7$ and $z = 9$ mm), the best results were obtained at an angle of 17.5 deg without taking into account the y and z coordinates.

The injector position change sensitivity range was determined to be:

$$delta\ y = 0.5(\max(y(i)z(j)alpha(k)) - \min(y(i)z(j)alpha(k)))$$

where the values max() and min() can be found in Fig. 10 (i, j, k are the same as in Eq. 2–10).

The results of these calculations can be seen in Fig. 12. It follows that the results are most sensitive to the y coordinate injector position change.

Another variable determining the total index sum value (expressed in numerical form in Fig. 12) is the change in distance from the axis of the spark plug. The least sensitive parameter for changes in fuel atomization indicators is the injector angle.

7 Conclusions

Injector location tests were performed using computer simulation, which were used to analyze the combustion process indicators. The best solution was defined as one which allowed to obtain the largest value of the sum of all these indicator values.

The pseudo-optimal location (within the adopted model boundaries), was characterized by:

- the largest inset in the combustion chamber y = 7 mm,
- the shortest distance from the spark plug $z = 9$ mm,
- the highest angle in relation to the axis of the cylinder alpha = 20 deg.

The maximum changes in thermodynamic indicators of fuel injection for different parameter changes:

- evaporated fuel mass (max – 7.4% for injector inset; min - 1.1% for injector angle),
- unevaporated fuel mass (max – 18.9% for injector inset, min – 2.7% for injector angle),
- droplet diameter (max – 6.8% for injector distance from the spark plug, min – 2.6% for injector angle),
- turbulence kinetic energy (max – 7.1% for injector inset. min - 0% for injector angle),
- energy dissipation (max – 7.1% for injector inset, min – 0.1% for injector angle)
- excess air ratio (max – 7.5% for injector inset, min – 1.1% for injector angle).

The maximum changes in thermodynamic indicators of combustion process for different parameter changes:

- maximum temperature (max – 4.2% for injector inset; min – 1.6% for injector distance from the spark plug),
- maximum pressure (max – 11.9% for injector angle, min – 4.1% for injector distance from the spark plug),
- total heat released (max – 3.9% for injector inset, min – 0.9% for injector distance from the spark plug),
- NO concentration (max – 33.7% for injector angle. min – 7.8% for injector inset),
- soot concentration (max – 160.3% for injector angle, min – 3.3% for injector distance from the spark plug)
- CO_2 concentration (max – 3.5% for injector angle, min - 0.7% for injector distance from the spark plug).
- CO concentration (max – 12.6% for injector inset, min – 3.2% for injector angle).

Sensitivity of changes to the injector position was determined based on the total indicator sum of changes in a given coordinate or angle (Fig. 11). The analysis of this sensitivity leads to the following conclusions:

- the longitudinal change of the injector position is the most important parameter affecting changes in the fuel atomization and combustion process indicators;
- this effect is about 3 times more significant than changes caused by the adjustment of the injector's distance from the spark plug axis and about 8 times more significant than the angle of the injector's position.

The conclusions obtained after the simulation analysis of the phenomenon will be taken into account in comparison of fuel atomization rates in the two injectors system and during combustion process analysis of such system.

8 Acknowledgements

The research was conducted using the AVL Fire software thanks to the AVL University Partnership Program.

References

Zimmerman, N.; Wang, J. M.; Jeong, C.-H.; Wallace, J. S.; Evans, G. J. *Environmental Science & Technology* **2016**, *50*, 8385–8392.

Pielecha, I. *International Journal of Automotive Technology* **2014**, *15*, 47–55.

Fiengo, G.; di Gaeta, A.; Palladino, A.; Giglio, V. *Common Rail System for GDI Engines*; Springer London, 2012; pp 17–33.

Zulkefli, M. H.; Mansor, M. R. A. The effect of injector position on direct injection hydrogen engine conditions. 2015.

Chintala, V.; Subramanian, K. *Energy* **2013**, *57*, 709–721.

Chen, Z.; Yao, C.; Yao, A.; Dou, Z.; Wang, B.; Wei, H.; Liu, M.; Chen, C.; Shi, J. *Fuel* **2017**, *191*, 150–163.

Yan, B.; Wang, H.; Zheng, Z.; Qin, Y.; Yao, M. *Applied Thermal Engineering* **2018**, *129*, 199–211.

Altin, I.; Bilgin, A. *Applied Thermal Engineering* **2015**, *87*, 678–687.

Ravi, K.; Porpatham, E. *Applied Thermal Engineering* **2017**, *110*, 1051–1060.

Gonca, G. *Applied Thermal Engineering* **2017**, *127*, 194–202.

Gupta, S. K.; Mittal, M. *Applied Thermal Engineering* **2019**, *148*, 1440–1453.

Nazemian, M.; Neshat, E.; Saray, R. K. *Applied Thermal Engineering* **2019**, *152*, 52–66.

Ahmadi, R.; Hosseini, S. M. *Applied Energy* **2018**, *213*, 450–468.

Krishnaraj, J.; Vasanthakumar, P.; Hariharan, J.; Vinoth, T.; Karthikayan, S. *Materials Today: Proceedings* **2017**, *4*, 7903–7910.

Ranga, A. P. R.; Surnilla, G.; Thomas, J.; Sanborn, E.; Linenberg, M. Adaptive Algorithm for Engine Air – Fuel Ratio Control with Dual Fuel Injection Systems. SAE Technical Paper Series. 2017.

Wiemann, S.; Hegner, R.; Atakan, B.; Schulz, C.; Kaiser, S. A. *Fuel* **2018**, *215*, 40–45.

Akansu, S. O.; Tangöz, S.; Kahraman, N.; İlhak, M. İ.; Açıkgöz, S. *International Journal of Hydrogen Energy* **2017**, *42*, 25781–25790.

García-Morales, J.; Cervantes-Bobadilla, M.; Escobar-Jimenez, R.; Gómez-Aguilar, J.; Olivares-Peregrino, V. *International Journal of Hydrogen Energy* **2017**, *42*, 25026–25036.

Liu, K.; Li, Y.; Yang, J.; Deng, B.; Feng, R.; Huang, Y. *Applied Energy* **2018**, *212*, 13–32.

Su, T.; Ji, C.; Wang, S.; Cong, X.; Shi, L. *International Journal of Hydrogen Energy* **2018**, *43*, 1902–1908.

Kosmadakis, G.; Rakopoulos, D.; Rakopoulos, C. *International Journal of Hydrogen Energy* **2015**, *40*, 15088–15104.

Ghadimi, P.; Yousefifard, M.; Nowruzi, H. *Journal of Applied Fluid Mechanics* **2016**, *9*, 2781–2790.

Reitz, R. D.; Beale, J. C. *Atomization and Sprays* **1999**, *9*, 623–650.

Sidorowicz, M.; Pielecha, I. *Combustion Engines* **2018**, *172*, 35–43.

Maroteaux, F.; Saad, C. *Energy* **2015**, *88*, 515–527.

Tan, J. Y.; Bonatesta, F.; Ng, H. K.; Gan, S. *Applied Thermal Engineering* **2016**, *107*, 936–959.

Petrakides, S.; Butcher, D.; Pezouvanis, A.; Chen, R. *Journal of Power Technologies* **2018**, *98(5)*.